JOURNAL OF SPACECRAFT AND ROCKETS
Vol. 43, No. 6, November–December 2006

Stochastic Spacecraft Thermal Design Optimization with Low Computational Cost

Issamu Muraoka,* Roberto L. Galski,† Fabiano L. de Sousa,‡ and Fernando M. Ramos§
National Space Research Institute, 12201-970 São José dos Campos, Brazil

DOI: 10.2514/1.20066

This paper presents a strategy for a quick determination of the optimum configuration for radiators and solar absorbers in a spacecraft thermal design, to minimize heater power consumption and maximize temperature margins. It is particularly useful when applied to multimission platforms in which the thermal design is adapted for different orbits and operational modes. A two-step approach is adopted wherein a simplified thermal model is developed to search for the optimum radiator/solar absorber areas, and then the results are implemented in a detailed thermal model to verify the temperature distribution, thereby reducing computational time, a common drawback in complex engineering optimization problems. If necessary, small adjustments are then made in the radiator/solar absorber configuration. The search for the optimum design is accomplished using a recently proposed global search metaheuristic, called generalized extremal optimization. Based on a model of natural evolution, it is easy to implement and has only one free parameter to adjust, making no use of derivatives. This paper presents the strategy as applied to the thermal design of the Brazilian Multimission Platform now under development.

Nomenclature

A_i	=	area of the radiator or solar absorber of node i, m^2
a	=	weighting factor for heater power consumption
b_l	=	weighting factor for temperature deviation for critical case l
F_{ij}	=	view factor between nodes i and j
f	=	objective function
G_{ij}	=	conductive conductance between nodes i and j, W/K
k	=	rank of the bit
L	=	number of bits used to encode the design variables
N	=	number of design variables
nc	=	number of critical cases
nn	=	number of nodes in the simplified model
P_k	=	probability of bit mutation
Q_i	=	internal heat dissipation on node i, W
Qh_i	=	heater power on node i, W
qir_i	=	incident Earth radiation density on node i, orbit average, W/m^2
qs_i	=	incident solar radiation density on node i, orbit average, W/m^2
R_{ij}	=	radiative conductance between nodes i and j, W/K^4
T_i	=	temperature of node i, K
$\boldsymbol{T}_l$	=	temperature vector for critical case l, K
$\boldsymbol{TT}$	=	target temperature vector, K
X	=	optimization variable
$\boldsymbol{X}$	=	optimization variable vector
$\boldsymbol{X}_{\text{best}}$	=	optimization variable vector that gives the best objective function value
α	=	solar absortivity
ΔT_{margin}	=	temperature design margin, K
ε	=	infrared emissivity
τ	=	optimization control parameter
τ^*	=	best value for the optimization control parameter

Subscripts

abs	=	solar absorber
CC	=	cold case
HC1	=	hot case 1
HC2	=	hot case 2
i, j	=	node, equipment box or panel
ibit	=	bit
l	=	critical case
min	=	lower limit
max	=	upper limit
rad	=	radiator
sp	=	solar panel
∞	=	space

Received 14 September 2005; revision received 19 June 2006; accepted for publication 30 June 2006.

*Research Engineer, Space Mechanics and Control Department, Av. dos Astronautas, 1758; issamu@dem.inpe.br.

†Research Engineer, Satellite Tracking and Control Center; galski@cc-s.inpe.br.

‡Research Engineer, Space Mechanics and Control Department; fabiano@dem.inpe.br.

§Senior Researcher, Applied Computational Laboratory; fernando@la-c.inpe.br.

I. Introduction

SATELLITES orbiting the Earth receive heat loads on their external surfaces from 1) direct solar radiation, 2) solar radiation reflected from Earth (albedo) and 3) infrared (IR) radiation emitted from Earth. Moreover, some of the onboard equipment dissipates electrical power, producing additional heat. Both external and internal heat loads vary according to the satellite orbit and attitude, the equipment operation modes, and the environmental conditions. Inside the satellite, the heat exchange modes are conduction and radiation. The balance among the heat input to the satellite, the outgoing heat to space from the external surfaces, and the internal heat exchange is what determines the temperature distribution within the satellite body.

The aim of the thermal design of a satellite is to keep all its components within their specified temperature range. The common design approach is to use a combination of multilayer insulation (MLI) blankets, radiators, solar absorbers, and electrical heaters. The satellite body is insulated from the space environment by wrapping it with MLI blankets. Some areas, called radiators, are left without blankets and covered with a high IR emissivity coating, so that they can irradiate the heat generated internally into space. Other areas, called solar absorbers, also without blankets, are covered with a high solar absortivity coating to keep warm the cold sensitive components. Heaters are used to control the temperature of some thermal sensitive equipment such as battery and propulsion subsystem components.

The radiators and solar absorbers are sized in a way to satisfy the thermal requirements of all components and also to minimize the power consumption of the active heaters. Defining the areas of the satellite radiators and solar absorbers is a time-consuming task, mainly when there are several areas available and a large number of possible combinations exists. The search for an acceptable radiator/solar absorber configuration is an interactive process, usually driven by previous experience. Once a satisfactory solution is reached, a question always arises: is it the best configuration? That is to say, is this configuration the one that yields minimum consumption of the heater power and maximum temperature margins for the equipment? Frequently, due to tight schedules, once the proposed design satisfies the temperature requirements and the heater's power budget, no additional effort is spent in the optimization process.

Past thermal design optimization strategies have proposed finding the optimum solution through the derivatives of an objective function with respect to design variables [1,2]. They failed, mainly due to the high computation time required and the inadequacy of the optimization method for this type of problem. More recently, with the advances in computer technology, new optimization techniques have been proposed.

Fragnito et al. [3] describe a procedure focused mainly on optimizing the thermal design of the solar panels of a microsatellite. It is based on successive model size increases and a parametric optimization strategy. Martin [4] presents a thermal analysis tool for the worst-case determination and design optimization. In this case, a gradient-based optimization method is adopted, combined with a latin hypercube method, so that the chance of finding the global optimum can be improved. This technique is useful when applied to small and simple models, suitable for the early stages of the thermal design process. When applied to a detailed model, the computational demand is too high.

Mareschi et al. [5], Herrera and Sepúlveda [6], and Lamela and Torres [7] propose the application of a stochastic analysis to improve the thermal design. A correlation matrix is generated by running a number of simulations with random samples of the design variables. It is used directly by the thermal analyst to improve the design [5,6] or as an input for an automatic search of the optimum solution [7]. The stochastic algorithm is implemented using the parallel virtual computer concept that allows it to tackle detailed design optimization, but demands an appropriate computational resource.

This paper presents a strategy that is applicable at an advanced stage of the thermal design process, to determine the optimum configuration of the radiator/solar absorber, using small computational resources. The idea is to use two mathematical models, taking advantage of a simplified model for optimization and of a detailed model to achieve the final design. Thus, the optimum solution is reached in two steps. Initially, the optimum radiator/solar absorber areas are obtained using a new stochastic algorithm called generalized extremal optimization (GEO) [8–10]. It is applied to a simplified thermal model especially developed to reduce the computation time in the optimization process. Next, the shapes of the radiator/solar absorber are defined and implemented in a detailed thermal model, using the optimum areas as inputs. Whenever necessary, small adjustments are made to reach the final design. In this strategy, the simplified model and the constraints for the optimization are conveniently built in such a way that the results obtained from are close to being the final optimal design solution.

The proposed strategy is especially useful when applied to multimission platforms in which a similar satellite configuration is adapted to different orbits and operational modes. The strategy outlined in this paper was tested on the Brazilian Multimission Platform (MMP) spacecraft [11]. It is a multipurpose space platform to be used in different types of missions, such as Earth observation, scientific or meteorological data collecting.

II. Proposed Optimization Strategy

The satellite thermal modeling involves several tasks. First, the satellite data (geometrical, thermal, orbital, and attitude) are preprocessed and transformed into a system of differential equations, which represents the thermal behavior of the satellite in orbit. Most of the thermal analyses are performed assuming steady-state conditions with orbit average heat loads. In this case, the system of differential equations is reduced to a system of nonlinear algebraic equations. The solution of this system results in the temperature distribution. Generally, the preprocessing consumes far more computing time than the numerical solution of the system of equations.

In the traditional design approach, the thermal analyst searches for an acceptable thermal design interactively by solving the direct problem. That means that the temperatures are calculated for each candidate configuration, following the sequence indicated in the preceding paragraph.

The optimization process is an inverse problem in which a thermal design configuration is sought for a desired temperature distribution. In this process, the direct problem is solved several times. If a large model is used, the computing time becomes too long and the optimization process impracticable, unless high-power computational resources are available.

In the proposed strategy for the optimization of the radiator/solar absorber configuration, a simplified thermal model is developed and used to obtain the optimum radiator/solar absorber areas with reduced computation time. The shapes are defined in a subsequent step. The detailed thermal model is used only at the end of the process to check the obtained solution and to make small adjustments, if necessary.

The design variables are explicit in the system of equations formulated for the simplified model. This saves a lot of computing time, because there is no need to perform the preprocessing tasks every time the design variables are changed. To have the design variables explicit in the system of equations, some assumptions are made: 1) the external MLI blankets are ideal, that is, the surfaces covered with the blankets are ideally insulated; 2) any changes in the radiator/solar absorber areas do not affect the view factor between them and other surfaces; 3) there is no multireflection of radiation between radiator/solar absorber and other surfaces; and 4) the incident external radiation is considered uniform over each external panel. As the MLI blankets are actually an excellent insulator, the effect of assumption 1 is small. Assumptions 2–4 will degrade the temperature calculation only if there are surfaces in front of the radiators or solar absorbers. The smaller the shape factor between radiator/solar absorber and other surfaces, the smaller will be the corresponding errors.

To obtain a simplified model, the well-known technique of merging the equipment boxes with the respective mounting panel is adopted. This means that just one temperature is determined for a whole panel. Because the equipment boxes are not represented individually, the equipment temperature limits cannot be used directly. New ones are determined for each panel, taking into account the most restrictive limit among the equipment boxes assembled on the panel and considering the thermal gradient between the boxes and the panel, that is,

$$T_{\min,i} = \max[(T_{\min,j} - Q_{\min,j}/G_{j,i}), j = 1, n] + \Delta T_{\text{margin}} \qquad (1)$$

$$T_{\max,i} = \min[(T_{\max,j} - Q_{\max,j}/G_{j,i}), j = 1, n] - \Delta T_{\text{margin}} \qquad (2)$$

where j represents the equipment box mounted on panel i, n is the number of equipment boxes on panel i, and ΔT_{margin} is the design margin established by the satellite program.

The optimization algorithm coupled to the solver automatically searches for the optimum radiator/solar absorber areas, using the simplified model and considering all critical cases, that is, the ones that pose extreme thermal conditions to the satellite. The objective is to minimize the power consumption of the heater and the temperature excursions, constrained by the panel temperature limits calculated by Eqs. (1) and (2). Mathematically, the multi-objective problem of minimizing the heater power and the differences between the target and the calculated temperatures is formulated as a mono-objective optimization problem, applying weighting factors for each objective:

Minimize

$$f(\boldsymbol{X}) = a \max\left[\left(\sum_{i=1}^{nn} Qh_i\right)_l, l = 1, nc\right] + \sum_{l=1}^{nc} b_l \|\boldsymbol{T}_l(\boldsymbol{X}) - \boldsymbol{TT}\|_2 \tag{3}$$

Subject to:

$$\boldsymbol{X}_{\min} \le \boldsymbol{X} \le \boldsymbol{X}_{\max} \qquad \boldsymbol{T}_{\min} \le \boldsymbol{T}_l(\boldsymbol{X}) \le \boldsymbol{T}_{\max}, \qquad l = 1, nc$$

The first term of the objective function $f(\boldsymbol{X})$ computes the maximum heater power consumption among all critical cases and multiplies it by the weighting factor a. The second term is the Euclidean norm of the temperature deviation from the target value, for all critical cases, multiplied by the respective weighting factor, b_l. The target temperatures $\boldsymbol{TT}$ are defined as the midpoint of the allowable range.

Once the optimum radiator/solar absorber areas are obtained, they are transported to a detailed thermal model. The shapes of the radiator/solar absorber are molded according to the equipment layout on the panel. In this model, the satellite data are preprocessed to generate the system of equations, which is then solved to obtain the temperatures on all satellite equipment. The results obtained with the detailed model are then checked for constraint violations and adjustments are made, if necessary.

Some discrepancy between the models may occur because the simplified model is evidently limited in its accuracy. But the optimization using the detailed model would be impracticable in terms of computing time. So, the key to the success of such two-step approach lies in achieving a good tradeoff between computing time gain and low accuracy due to the simplified model. In the present study, the simplified model's accuracy can be verified when the results of the optimization are transported to the detailed model. The proximity between the temperatures and heater power consumption as calculated by the simplified model and the ones obtained with the detail model is a good indication of the fidelity of the simplified model. The accuracy of the detailed model, in turn is verified/adjusted experimentally through a thermal balance test [12].

III. Optimization Algorithm

The generalized extremal optimization algorithm is a global search metaheuristic [8–10] based on a model of natural evolution [13]. GEO is a stochastic method especially devised to be used in complex optimization problems [14,15]. It does not use derivatives and can be applied to nonconvex or disjoint problems. It can also deal with any kind of variable: continuous, discrete, or integer. An a priori advantage of GEO over other metaheuristics like simulating annealing (SA) and genetic algorithms (GAs), is that it has only one free parameter to adjust.

GEO is an evolutionary algorithm where species are represented by bits of a string that encodes the design variables. Thus, each bit is considered a species. A fitness number is associated to each bit, according to the gain (or loss) the objective function value has when the bit is mutated (flipped). All bits are then ranked from the least to the best adapted. A bit is then mutated according to the probability distribution $P_k \approx k^{-\tau}$, where k is the rank of a selected bit candidate to mutate, and τ is a free control parameter. If $\tau \to 0$, then any bit has the same probability to be mutated, whereas for $\tau \to \infty$, only the least adapted bit will be mutated. It has been observed that the best value of τ for a given application (τ^*, i.e., the one that yields the best performance of the algorithm on the application at hand) generally lies within the range [1, 5], which makes the setting of τ a relatively easy task.

A variant of the standard GEO exists wherein 1 bit per variable is mutated at each iteration of the algorithm. In this case, the ranking is done separately for each design variable. In this study the standard GEO was used because it has been observed that it is more efficient for highly constrained problems, such as the one dealt with here. A flowchart of the standard GEO is shown in Fig. 1.

The algorithm is initialized in Step 1 by randomly setting the values of the bits on the string. In Step 2 the fitness attributed to each bit is given by $\Delta f(\boldsymbol{X})_{\text{ibit}} = [f(\boldsymbol{X})_{\text{ibit}} - f(\boldsymbol{X})_{\text{best}}]$, where $\boldsymbol{X}$ is the vector of variables calculated from the bit string, $f(\boldsymbol{X})_{\text{ibit}}$ is the value of the objective function if the bit ibit is flipped, and $f(\boldsymbol{X})_{\text{best}}$ is the best value of the objective function found so far at the beginning of Step 2. Note that in this step, after the value of $\Delta f(\boldsymbol{X})_{\text{ibit}}$ is calculated, the bit is returned to its original value. In Step 3 the bits are ranked from $k = 1$, for the least adapted one, which is equivalent to the least value of $\Delta f(\boldsymbol{X})_{\text{ibit}}$ in a minimization problem, to $k = L$ for the best adapted one. In Step 4 a candidate bit is chosen randomly to mutate and the value of P_k is calculated, where k is the value of the rank of the chosen candidate bit. If $P_k \ge \text{RAN}$ (a randomly generated number in the interval [0, 1]), the bit is accepted to mutate. This process is repeated until a bit is confirmed to mutate.

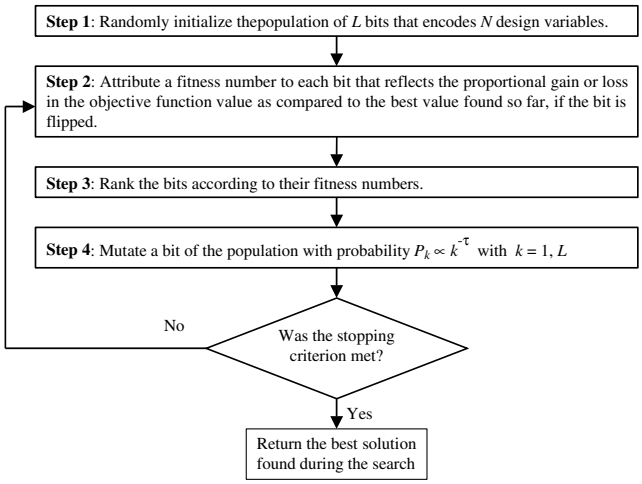

Fig. 1 Flowchart for GEO.

The criterion to stop the run is chosen according to the problem being solved. For example, a maximum processing time or maximum number of function evaluations can be used. For the present application the maximum number of function evaluations criterion was adopted.

Constraints are easily taken into account in GEO. Boundary constraints are incorporated directly by the binary encoding. Inequality and equality constraints are taken into account by assigning a high fitness for the bit that, when flipped, leads the algorithm to an unfeasible region of the design space. Note that this move is not prohibited, it only has a low probability of happening. In fact, the algorithm can even be initialized from an unfeasible design.

A detailed explanation of the algorithm, including application examples and performance comparisons with other stochastic algorithms, can be found in [9,10].

IV. MMP Satellite

The Multimission Platform (MMP) is a multipurpose space platform to be used in different types of missions such as Earth observation, scientific or meteorological. The MMP is a concept of satellite architecture that consists of assembling all equipment essential to the satellite on a single platform, regardless of the payloads it eventually will carry. In this kind of architecture, there is a physical separation between the platform and the payload module, which can be developed, manufactured, and tested separately, before the last phases of integration and testing. Additionally, it has the advantage of reusing the platform design for new satellites, resulting in lower development costs. Table 1 presents the general characteristics of the MMP and Figs. 2 and 3 show its physical configuration. The heat dissipation and temperature limits for the equipment are listed in Table 2.

The thermal control concept is based on passive means with the following baseline design: 1) the external surface of panels −Y, +X, +Y, and −X are covered with MLI blankets, leaving some areas for thermal radiators; 2) the external surface of panel −Z is covered with MLI blankets, leaving some area for a solar absorber because this

Table 1 MMP characteristics

Characteristics	Value
Dimensions	$1 \times 1 \times 1$ m^3
Mass	250 kg
Power consumption	250 W
Power supply to payload	170 W
Orbit inclinations	Near equatorial ($i < 15$ deg) and sun-synchronous
Orbit altitudes	600–1200 km
Attitude	Earth, sun, or inertial-pointing
Maneuver capabilities	$\Delta V = 150$ m/s
Data storage capability	2 Gbits

panel supports the hydrazine tank, lines, and valves that must be kept warm to avoid hydrazine freezing; 3) all internal surfaces are painted black, except the battery panel and propulsion components (hydrazine tank, tubing, and valves) that are covered with MLI blankets; 4) propulsion components are conductively insulated from the mounting panel (panel −Z); 5) the battery panel is conductively insulated from the rest of the platform; 6) the platform is thermally insulated from the payload module, and 7) heaters are used for temperature control of the batteries and propulsion components.

Whereas this basic thermal design approach is common to all MMP missions, the radiator and absorber configurations on −Y, +X, +Y, −X, and −Z panels may be modified for each specific mission to meet the mission's temperature requirements.

V. Thermal Mathematical Model

Thermal models of satellites are usually developed using a lumped parameter network formulation [16]. In this method, the satellite is divided into a number of lumped masses, called nodes, which are assumed isothermal. A thermal network is drawn, connecting the nodes. A governing thermal energy expression is written for each node, resulting in a system of coupled equations whose solution yields their temperatures. For the MMP, the thermal model was constructed using the PCTER thermal software package [17]. This package, developed indigenously for the Brazilian satellite program, covers the whole cycle of satellite thermal analysis tasks, including calculation of view factor, radiative and conductive conductances, external radiation fluxes, and steady-state and transient temperatures.

To apply the proposed optimization technique, a simplified lumped parameter model was constructed for the MMP, using nine nodes (six for the platform side panels, two for the solar panels, and one for the propulsion components, as defined in Table 2). The equipment boxes were merged to their respective mounting panels. The internal heat dissipation on each panel was defined as the summation of the heat dissipation of the equipment mounted on it.

The allowed temperature range for each panel was calculated, using Eqs. (1) and (2), considering a design margin of 5 K. The data for calculation and the results are presented in Table 2.

According to the architecture, the six MMP panels exchange heat among themselves by conduction and/or radiation (through the inner surfaces). They also exchange heat, by radiation, with the space environment through the outer surfaces. Nodes 3 (+X panel) and 5

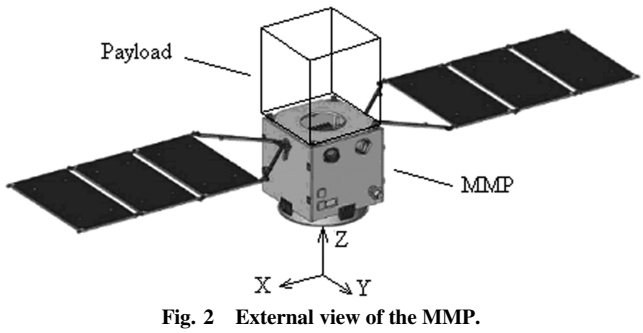

Fig. 2 External view of the MMP.

Table 2 Equipment and node data

Panel i	Equipment data				Node data				
	Equipment j	Max dissip., W	Min dissip., W	Allow temp., K	G_{ji}, W/K	Node	Max dissip., W	Min dissip., W	Allow temp., K	Target temp., K
−Z	Reac. wheel (nos. 1, 2, 3)	3 × 3.8	3 × 2.9	258–338	0.63	1	11.4	8.7	260–330	295
	Reac. wheel no. 4	0	0	258–338	0.63					
−Y	Battery (nos. 1, 2, 3, 4)	4 × 2.8	4 × 2.0	263–293	1.33	2	12.0	8.0	266–286	276
	Magnetotorquer no. 1	0.8	0	243–338	7.9					
+X	OBC	61	49	263–313	18.9	3	73.7	58.7	265–305	285
	GPS	4.7	4.7	253–333	3.00					
	SADA no. 1	5	5	253–333	0.88					
	Magnetotorquer no. 2	3	0	243–338	7.9					
+Y	Inertial unit no. 1	0	0	243–343	6.49	4	5.08	26	257–310	284
	Star sensors (nos. 1, 2)	2 × 7.6	2 × 7.6	243–318	2.72					
	TT&C no. 1	29.2	4.4	243–323	4.90					
	TT&C no. 2	4.4	4.4	253–323	4.90					
	Magnetometer (nos. 1, 2)	2 × 1	2 × 1	234–349	0.88					
−X	PCDU	39	10	263–318	12.0	5	78.0	46.0	267–310	289
	Inertial unit no. 2	31	31	243–343	6.49					
	SADA no. 2	5	5	253–333	0.88					
	Magnetotorquer no. 3	3	0	243–338	7.9					
+Z	No equipment	——	——	——	——	6	0	0	258–318	288
−Z	Propul. components	——	——	283–323	——	7	0	0	288–318	303
+X solar p.	No equipment	——	——	——	——	8	0	0	193–353	——
−X solar p.	No equipment	——	——	——	——	9	0	0	193–353	——
	Total	225.9	147.4				225.9	147.4		

(−X panel) exchange heat also with the solar panels (nodes 8 and 9 in Table 2).

The MLI blankets covering the external surfaces of the six panels were considered ideal. That is to say, theoretically, the six panels exchange heat with the space environment and with the solar panels only through the radiator and absorber areas.

Node 7, representing the propulsion components, was not modeled geometrically. It exchanges heat only by conduction with the −Z panel (node 1). The conductance is estimated by the summation of the conductances of all points of contact (bolted joints).

Using the lumped parameter representation [16] and assuming steady-state conditions with orbit average heat loads, the heat balance at each one of the nine nodes leads to the following equations:

$$\sum_{j=1}^{7} G_{1,j}(T_1 - T_j) + \sum_{j=1}^{6} R_{1,j}\left(T_1^4 - T_j^4\right) + A_1\varepsilon_{\text{abs}}\left(T_1^4 - T_\infty^4\right) = Q_1 + A_1(\alpha_{\text{abs}} qs_1 + \varepsilon_{\text{abs}} qir_1) \tag{4}$$

$$\sum_{j=1}^{6} G_{2,j}(T_2 - T_j) + \sum_{j=1}^{6} R_{2,j}\left(T_2^4 - T_j^4\right) + A_2\varepsilon_{\text{rad}}\left(T_2^4 - T_\infty^4\right) = Q_2 + A_2(\alpha_{\text{rad}} qs_2 + \varepsilon_{\text{rad}} qir_2) + Qh_2 \tag{5}$$

$$\sum_{j=1}^{6} G_{3,j}(T_3 - T_j) + \sum_{j=1}^{6} R_{3,j}\left(T_3^4 - T_j^4\right) + A_3\varepsilon_{\text{rad}}F_{3,\infty}\left(T_3^4 - T_\infty^4\right) + A_3\varepsilon_{\text{rad}}F_{3,8}\left(T_3^4 - T_8^4\right) = Q_3 + A_3(\alpha_{\text{rad}} qs_3 + \varepsilon_{\text{rad}} qir_3) \tag{6}$$

$$\sum_{j=1}^{6} G_{4,j}(T_4 - T_j) + \sum_{j=1}^{6} R_{4,j}\left(T_4^4 - T_j^4\right) + A_4\varepsilon_{\text{rad}}\left(T_4^4 - T_\infty^4\right) = Q_4 + A_4(\alpha_{\text{rad}} qs_4 + \varepsilon_{\text{rad}} qir_4) \tag{7}$$

$$\sum_{j=1}^{6} G_{5,j}(T_5 - T_j) + \sum_{j=1}^{6} R_{5,j}\left(T_5^4 - T_j^4\right) + A_5\varepsilon_{\text{rad}}F_{5,\infty}\left(T_5^4 - T_\infty^4\right) + A_5\varepsilon_{\text{rad}}F_{5,9}\left(T_5^4 - T_9^4\right) = Q_5 + A_5(\alpha_{\text{rad}} qs_5 + \varepsilon_{\text{rad}} qir_5) \tag{8}$$

$$\sum_{j=1}^{6} G_{6,j}(T_6 - T_j) + \sum_{j=1}^{6} R_{6,j}\left(T_6^4 - T_j^4\right) = 0 \tag{9}$$

$$G_{7,1}(T_7 - T_1) = Qh_7 \tag{10}$$

$$A_8\varepsilon_{\text{sp}}F_{8,3}\left(T_8^4 - T_3^4\right) + A_8\varepsilon_{\text{sp}}F_{8,\infty}\left(T_8^4 - T_\infty^4\right) = A_8(\alpha_{\text{sp}} qs_8 + \varepsilon_{\text{sp}} qir_8) \tag{11}$$

$$A_9\varepsilon_{\text{sp}}F_{9,5}\left(T_9^4 - T_5^4\right) + A_9\varepsilon_{\text{sp}}F_{9,\infty}\left(T_9^4 - T_\infty^4\right) = A_9(\alpha_{\text{sp}} qs_9 + \varepsilon_{\text{sp}} qir_9) \tag{12}$$

The radiative conductances R_{ij}, for $i = 1$–6 and $j = 1$–6 (platform main body panels), are related to the radiation heat exchange among the internal surfaces of the panels. They were computed, using the preprocessor module of PCTER, assuming an emissivity of 0.85 (black paint) for nodes 1, 3, 4, 5, 6 and 0.05 (MLI blanket) for node 2.

To simplify the model, the radiative heat exchange between nodes 3 and 8 did not include multireflection. Furthermore, the view factors ($F_{3,8}$ and $F_{3,\infty}$) were calculated for the entire area of node 3. The same assumptions were adopted for the heat exchange between nodes 5 and 9.

The conductances G_{ij} (for $i = 1, 7$ and $j = 1, 7$) were determined from the characteristics of the bolted joints between the panels and the attachment fixture of the propulsion components on the −Z panel.

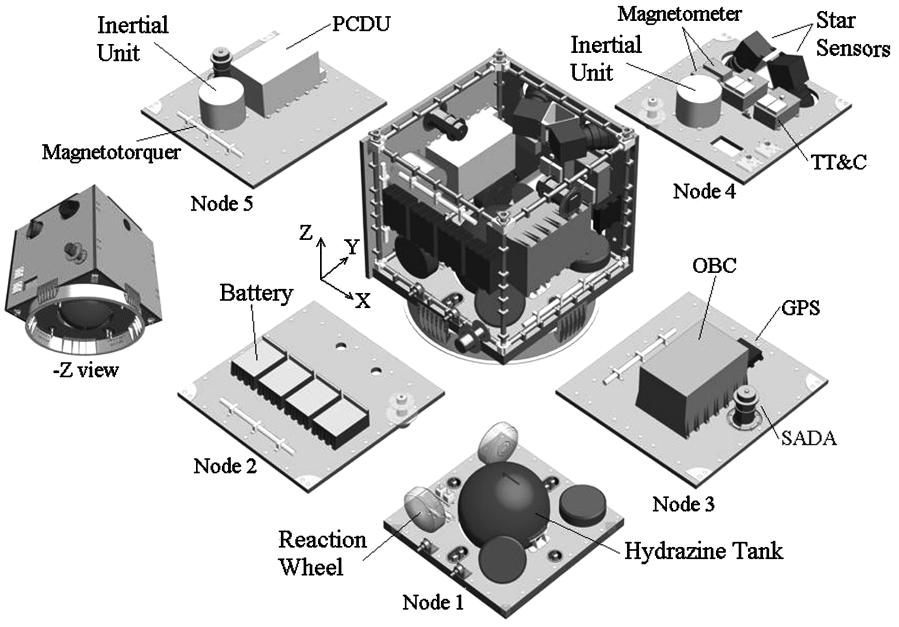

Fig. 3 Exploded view of the MMP.

Table 3 Missions analyzed

Characteristic	Mission 1	Mission 2
Orbit	Equatorial (inclination = ±15 deg)	Sun-synchronous passage time = 6:00 h
Altitude	600 km	1200 km
Orientation	−Y facing to Earth	−Y facing to Earth
Solar panel orientation	Perpendicular to orbit plane	Parallel to orbit plane
Beta angle range	−38– + 38 deg	57–103 deg
Period	5800 s	6560 s
Eclipse duration	1902–2129 s	0–269 s

The orbit average temperatures for a given environmental and operational mode were obtained by solving the system of algebraic equations.

VI. Missions Under Analysis

As an example of an application, two hypothetical missions with a MMP were selected. They are defined in Table 3 and illustrated in Figs. 4 and 5.

The satellite thermal design was based on the analysis of the critical cases that exposed the equipment to extreme thermal conditions. From the external environment point of view, three critical cases were identified for mission 1. The first one is a cold case (CC) that occurs when the sun is at the orbit plane (beta angle is 0 deg). It combines an orbit with a minimum direct solar illuminated period (maximum eclipse duration) with minimum satellite projected area to the sunlight. The two other cases are hot cases (HC1 and HC2). They occur when the beta angle is at its maximum and minimum values (+38 and −38 deg). They combine maximum illuminated period and maximum projected area to the sunlight. The three cases are illustrated in Fig. 4.

For mission 2, one cold and two hot critical cases were also identified. The cold case occurs when the beta angle is 90 deg. In this case, although the eclipse does not occur, there is no direct solar radiation incident on the MMP due to the shadow of the payload module. The two hot cases are very close to one another. The first one occurs when the beta angle is 57 deg, which corresponds to the minimum possible incidence angle of solar radiation on the MMP lateral panels (faces −X, +X, −Y, +Y), although the eclipse duration is merely 269 s. The second hot case is when the beta angle is 58 deg, which corresponds to the minimum incidence angle of solar radiation on the MMP lateral panels with no occurrence of eclipse. These critical cases are illustrated in Fig. 5.

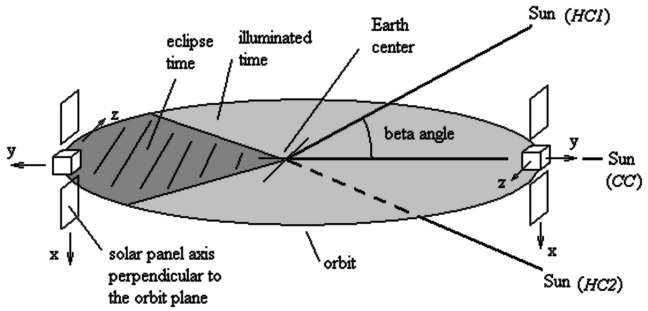

Fig. 4 Orbit and attitude for mission 1.

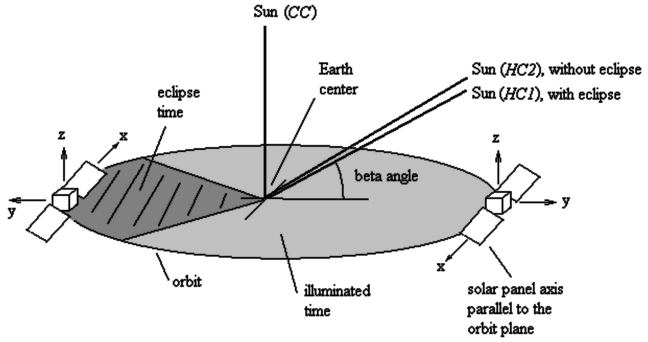

Fig. 5 Orbit and attitude for mission 2.

For each critical case, the average incident radiations (qs and qir) on each panel were calculated by the preprocessor module of PCTER, considering the extreme values of the following parameters: 1) solar constant ranging from 1326 to 1418 W/m^2, 2) albedo factor ranging from 0.20 to 0.28 for equatorial orbit and from 0.38 to 0.48 for sun-synchronous orbit, and 3) Earth radiation ranging from 233 to 265 W/m^2 for equatorial orbit and from 202 to 227 W/m^2 for sun-synchronous orbit. In addition to the external heat loads, the heat dissipation of the equipment inside the MMP was included, using the extreme values listed in Table 2.

VII. Formulation of the Optimization Problem

The objective of optimization was to determine the best combination of the radiator/solar absorber areas to minimize the heater power spent on the batteries and on the propulsion components and to maximize temperature margins, without violating the temperature constraints for all critical cases. The optimization variables are the absorber area of node 1 (A_1), the radiator areas of nodes 2 to 5 (A_2, A_3, A_4, A_5) and the heater power on node 2 (Qh_2) and 6 (Qh_6). They are represented by the vector $\boldsymbol{X}$[1:7] in the optimization process, as shown in Table 4.

For a given $\boldsymbol{X}$, the solution of the system of algebraic Eqs. (4–12) results in three sets of temperatures: $\boldsymbol{T}_{\mathrm{CC}}(\boldsymbol{X})$[1:9] for CC conditions, $\boldsymbol{T}_{\mathrm{HC1}}(\boldsymbol{X})$[1:9] for HC1 and $\boldsymbol{T}_{\mathrm{HC2}}(\boldsymbol{X})$[1:9] for HC2. The solution of the system of equations was obtained by the PCTER solver, which was coupled to the optimization algorithm.

Constraints were imposed on the node temperatures. The allowed range for each node was defined according to Eqs. (1) and (2), as presented in Table 2.

The objective was to minimize the heater power for battery and propulsion components and also to minimize the difference between the node temperature and a target temperature, defined as the midpoint of the respective allowable range (presented in Table 2). Derived from Eq. (3), the objective function was formulated as:

Minimize

$$f(\boldsymbol{X}) = X[6] + X[7] + 0.01\,\|\boldsymbol{T}_{\mathrm{CC}}(\boldsymbol{X}) - \boldsymbol{TT}\|_2 + 0.005\,\|\boldsymbol{T}_{\mathrm{HC1}}(\boldsymbol{X}) - \boldsymbol{TT}\|_2 + 0.005\,\|\boldsymbol{T}_{\mathrm{HC2}}(\boldsymbol{X}) - \boldsymbol{TT}\|_2 \tag{13}$$

Table 4 Variables for optimization

$\boldsymbol{X}$	Variable	Description	Allowable range
1	A_1	Absorber area on −Z panel (node 1)	0–0.1940 m^2
2	A_2	Radiator area on −Y panel (node 2)	0–0.8054 m^2
3	A_3	Radiator area on +X panel (node 3)	0–0.8054 m^2
4	A_4	Radiator area on +Y panel (node 4)	0–0.8054 m^2
5	A_5	Radiator area on −X panel (node 5)	0–0.8054 m^2
6	Qh_2	Heater power on batteries (node 2)	0–15 W
7	Qh_6	Heater power on prop. components (node 7)	0–15 W

Subject to:

$$\boldsymbol{X}_{\min} \le \boldsymbol{X} \le \boldsymbol{X}_{\max} \qquad \boldsymbol{T}_{\min} \le \boldsymbol{T}_{CC}(\boldsymbol{X}) \le \boldsymbol{T}_{\max}$$

$$\boldsymbol{T}_{\min} \le \boldsymbol{T}_{HC1}(\boldsymbol{X}) \le \boldsymbol{T}_{\max} \qquad \boldsymbol{T}_{\min} \le \boldsymbol{T}_{HC2}(\boldsymbol{X}) \le \boldsymbol{T}_{\max}$$

The weighting factors were chosen in a way to give high priority for heater power reduction and low priority for temperature centralization.

Note that the optimization of the radiator/absorber areas is performed simultaneously for the cold and hot cases, because the same design has to cope with all operational and environmental conditions expected to occur in orbit. This means that, in Eq. (13), whereas the area of each radiator is the same for the cold and hot cases, the heater power, variables $X[6]$ and $X[7]$, may assume different values for these critical cases. For the design of the MMP, they were set to zero in the hot cases and could vary only for the cold case.

VIII. Optimization Algorithm Setting

Stochastic optimization algorithms usually have adjustable parameters that must be properly set, so that they can work efficiently for a given application. One advantage of the GEO algorithm over other popular methods such as the GA and SA is that it has only one free parameter (τ) to be set. This makes the usually time-consuming task of parameter setting easier in GEO.

One way that may be used to choose τ is to perform preliminary searches with GEO, covering a range of τ values using a number of function evaluations, usually choosing about 10–20% of the total number to be considered later for the main searches. For the problem addressed here, τ^* was searched in the range $[0, 4.5]$ with steps of 0.5. For each τ, 25 runs were performed with 10,000 function evaluations each. The average of the best objective function values, $f(\boldsymbol{X}_{\text{best}})$, found in the 25 runs is shown in Fig. 6, as a function of τ. From this figure, it can be concluded that $\tau^* = 2.0$. This value was adopted for the main searches.

As for the setting of τ, in the main runs, each design variable was encoded in 4 bits resulting in a total of 28 bits ($L = 4$ bits/variable $\times$ 7 variables). The use of 4 bits per variable means a resolution of 0.0129 m^2 for the absorber area, 0.0537 m^2 for radiator areas, and 1.0 W for the heater power. Initially, a comparative test was performed using 7 and 4 bits. The values of the optimum objective function obtained for both did not differ considerably, resulting in the choice of 4 bits, given its advantage of a smaller design space for the search. Moreover, using 4 bits, the resolution of the radiator (0.0537 m^2) coincided with the area of each node on the detailed model of the panel. With this, the optimum radiator areas were easily implemented into the detailed model.

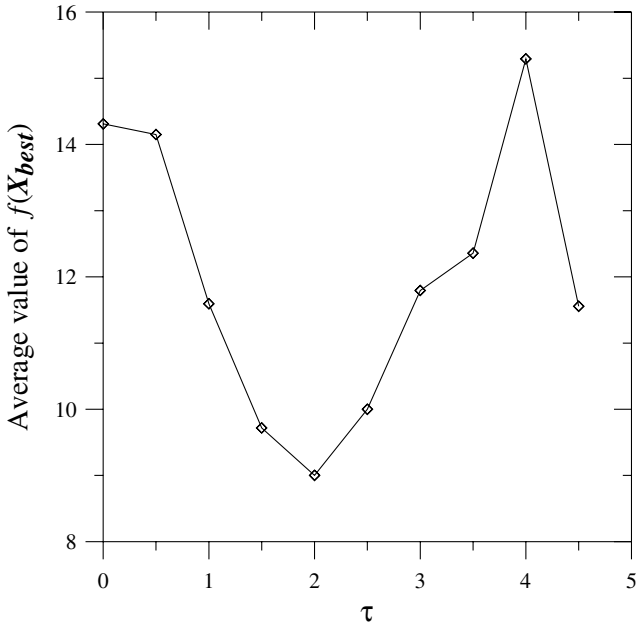

Fig. 6 Average of $f(\boldsymbol{X}_{\text{best}})$ as a function of τ.

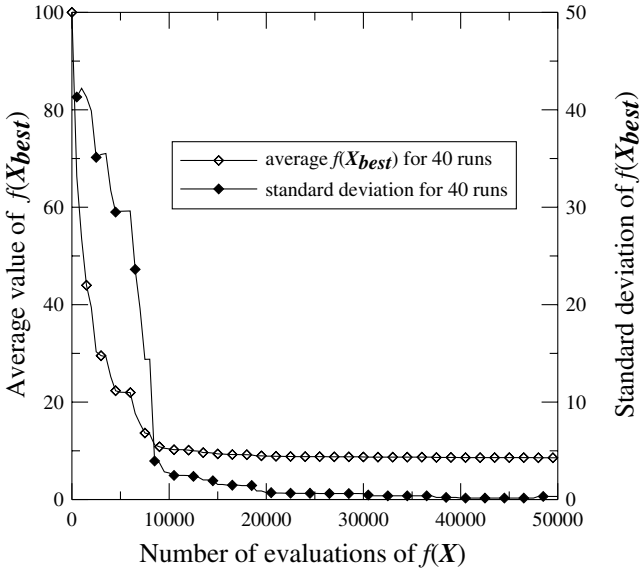

Fig. 7 Average value of $f(\boldsymbol{X}_{\text{best}})$ for 40 runs and its standard deviation.

For mission 1, the search for optimum radiator/solar absorber areas was done using 40 runs with 50,000 function evaluations each. In Fig. 7, the average $f(\boldsymbol{X}_{\text{best}})$ of the 40 runs and its standard deviation were plotted as a function of the number of evaluations. It can be seen that after approximately 20,000 function evaluations, there was a stagnation on the value of the average $f(\boldsymbol{X}_{\text{best}})$ and also on its standard deviation, that was also close to zero. This indicates that the global optimum was probably found. Moreover, it also indicates that, for this problem, the use of much more than 20,000 function evaluations in the same run would yield little, if any, improvement on the objective function. Hence, the stopping criteria was changed for the analysis of mission 2, where the algorithm was halted after 25,000 function evaluations for each run.

IX. Results

The best values found for the design variables and the objective function for missions 1 and 2 are presented in Table 5. The temperatures obtained with these solutions are presented in Figs. 8 and 9 for missions 1 and 2, respectively.

Considering the large number of objective function evaluations (2 million for mission 1 and 1 million for mission 2) and also the evolution of the objective function during the search, shown in Fig. 7, the possibility of having better solutions is small, and it is likely that the obtained configuration is, if not the best, at least one of the best solutions.

The optimum radiator/solar absorber areas were very sensitive to the orbital condition, as presented in Table 5. Although the heat dissipation of the equipment was the same for missions 1 and 2, the radiator/solar absorber areas and heater power consumption were

Table 5 Best solutions found for the two missions

Design variable	Mission 1	Mission 2
$X(1)$, m^2	0.1811	0.0777
$X(2)$, m^2	0.2685	0.2148
$X(3)$, m^2	0.2148	0.4296
$X(4)$, m^2	0.4296	0.1075
$X(5)$, m^2	0.1075	0.1612
$X(6)$, W	0	11
$X(7)$, W	6	8
$f(\boldsymbol{X})$	6.6436	19.7256

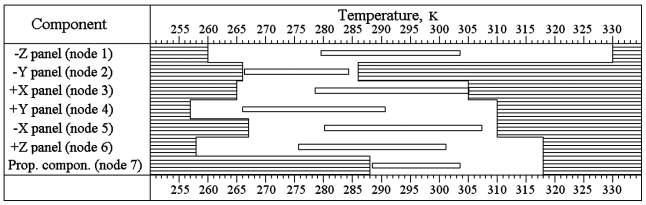

Fig. 8 Temperature excursion for mission 1.

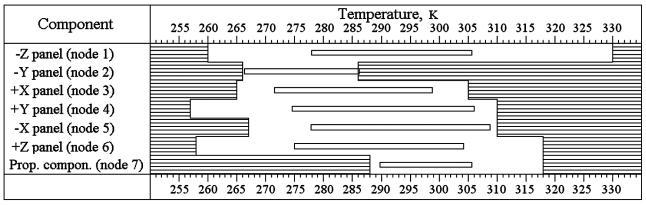

Fig. 9 Temperature excursion for mission 2.

very distinct. This result demonstrates how challenging it would be for the designer to make a "manual" search for the best radiator/solar absorber configuration.

Most of the predicted temperatures, as shown in Figs. 8 and 9, were not centered in the allowed range. This was a consequence of the formulation of the objective function that gave a higher priority to the reduction of the heater power (weight = 1) than to the temperature margin gain (weight = 0.01). It was assumed that an additional margin, above the 5 K considered in the calculation of the allowed range for the optimization process, was not as important as the reduction of the heater power.

The optimum radiator/solar absorber areas were obtained using the simplified model. The next step was to define the radiator/solar absorber shape and implement them in the detailed model.

The detailed model used the same lumped parameter method, but with a finer nodal breakdown. This model represents the MMP platform through 120 diffusion nodes and 124 arithmetic nodes, for a total of 244 nodes. Arithmetic nodes were used to represent the MLI blanket outer layers that have small mass. In Fig. 10, an external view of the nodal breakdown is depicted. In this model, each equipment box listed in Table 2 was represented by one node (not merged with the mounting panel as in the simplified model), thus allowing the calculation of each individual temperature.

The radiator/solar absorber shapes were defined according to the characteristics and the layout of the equipment boxes attached to the panel. The distribution of optimum radiator/absorber areas in the detailed model are presented in Figs. 11 and 12 for missions 1 and 2, respectively. Given the fact that in the optimization process, the resolution of the radiator area coincides with the node area of the detailed model, the task was simply to choose which nodes would work as radiators, but in certain occasions this was not possible. One such a case was the radiator on −Y panel. In this case, the optimum radiator area corresponds to five nodes, but, due to the layout of the batteries on this panel (as seen in Fig. 3), the radiator area was distributed to eight nodes (as seen in Fig. 11a).

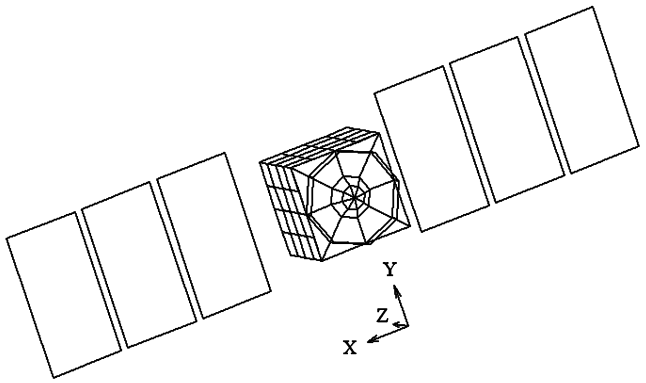

Fig. 10 Detailed model nodal breakdown.

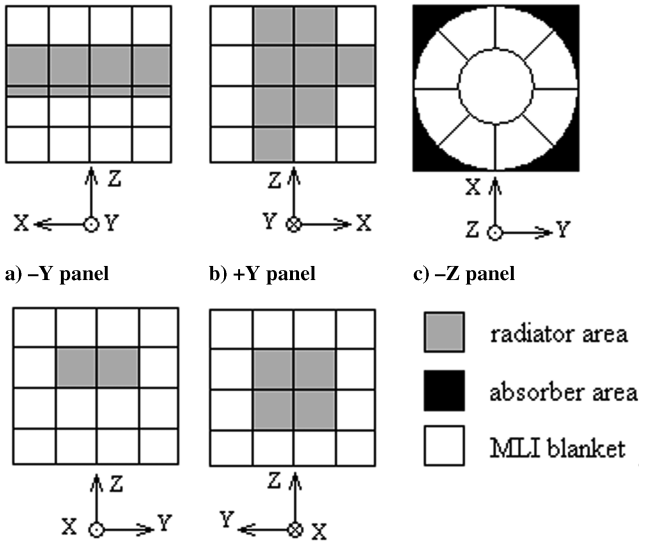

a) –Y panel **b) +Y panel** **c) –Z panel**

d) –X panel **e) +X panel**

Fig. 11 Radiator/solar absorber configurations for mission 1.

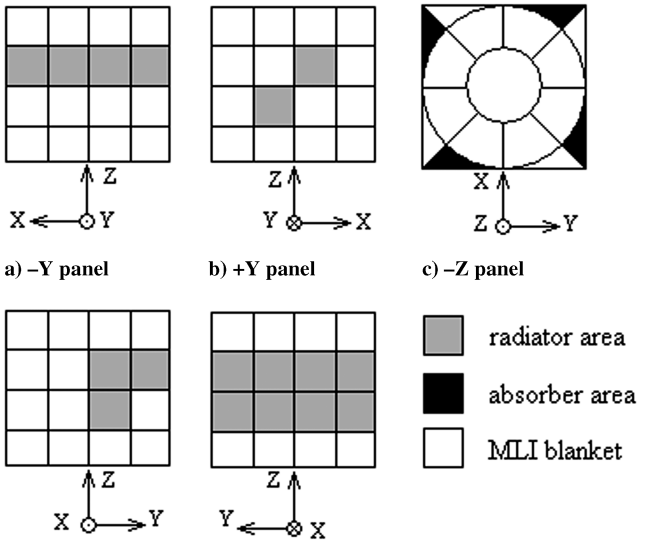

a) –Y panel **b) +Y panel** **c) –Z panel**

d) –X panel **e) +X panel**

Fig. 12 Radiator/solar absorber configurations for mission 2.

Once the radiator and solar absorber configurations were implemented in the detailed model, all preprocessing tasks were performed to obtain the system of equations. The solution of this system resulted in the temperatures of each equipment box, which are presented in Figs. 13 and 14 for missions 1 and 2, respectively.

The temperature prediction using the detailed model confirmed the results obtained by the simplified one in the optimization process, in most cases. That is to say, the temperature variation was within the required range in all but one equipment box. For mission 2, an adjustment was necessary in the heater power to warm the propulsion components. The heater power had to be increased from 8 to 13 W to keep the hydrazine tank above the minimum required temperature during the cold case.

X. Processing Time

To find the optimum radiator/solar absorber areas for mission 1, the objective function was evaluated two million times (40 runs with 50,000 evaluation each), consuming approximately 18 h of CPU of a PC AMD Athlon, 1.8 GHz clock, 256 MB RAM. For mission 2,

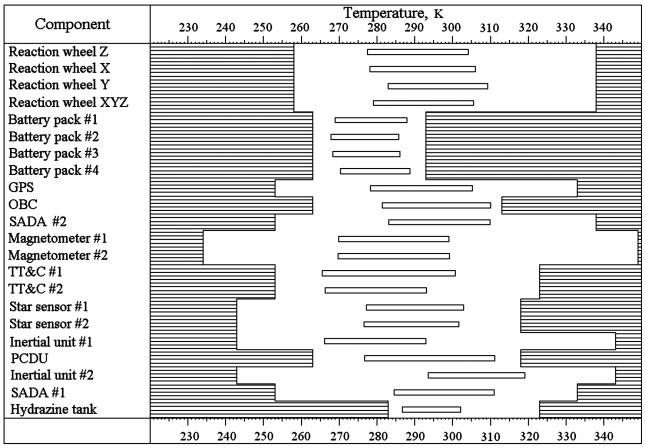

Fig. 13 Equipment temperatures for mission 1, obtained with the detailed model.

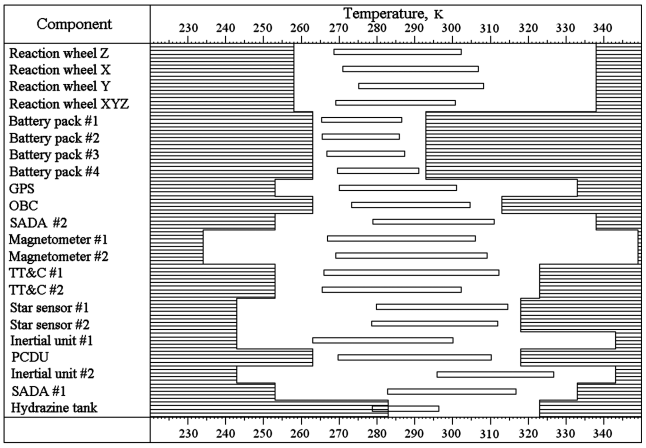

Fig. 14 Equipment temperatures for mission 2, obtained with the detailed model.

whose number of evaluations per run was reduced to 25,000, the processing time was around 6 h. Besides the time saved because of the reduction on the number of evaluations, the large reduction of the processing time for the mission 2 was due to the fact that in this mission there were fewer viable solutions. Each set of design variables was tested for the critical cases in a sequence. If the temperatures calculated for a given critical case (the cold case, for example) were out of the allowed range, this set of variables was discarded without testing for the remaining critical cases (two hot cases). This means that if the viable space was small, less critical cases were tested.

If the detailed model had been used for the optimization process, the following sequence of operations, with the respective processing time using the same computer, would be necessary to obtain the temperatures for each critical case: 1) calculation of radiative coupling for external surfaces (19 s); 2) calculation of solar, albedo, and Earth radiation on the external surfaces (6 min 56 s); and 3) solving the system of equations (2 s). The total processing time would then be 7.28 min. Supposing just one critical case and considering the same number of function evaluations used in mission 2, the optimization process would take around 7,280,000 min or 5055 days, making it nearly impossible to solve the problem.

XI. Conclusion

A stochastic strategy for satellite thermal design to determine the optimum radiator and solar absorber configurations, while minimizing heater power consumption, was presented. This strategy was developed to be used in problems where the optimization of the detailed thermal model would require a prohibitive computational cost. It is especially useful for the analysis of multimission platforms which, by definition, are designed for different orbital conditions and operational modes.

The approach presented comprised two main steps: 1) to develop a simplified thermal model to search for the optimum radiator and solar absorber areas, using a stochastic algorithm: a novel metaheuristic called generalized extremal optimization algorithm; and 2) given the optimum areas, to define the radiator and solar absorber shapes according to the equipment layout and to implement them in the detailed model, then making final adjustments, if necessary.

This strategy was applied to the thermal design of the Brazilian Multimission Platform for two hypothetical missions. The optimum radiator/solar absorber configuration was quickly determined for both missions with low computational and analysis cost. Considering the large number of objective function evaluations and also the insights obtained during the optimization process, it is likely that the obtained configuration is close to the best solution in terms of heater power consumption and temperature margins.

The main difficulty of this two-step strategy is to develop a simplified model that has a good correlation with the detailed model. The small number of nodes and the assumptions adopted to characterize the physical components of the spacecraft in the simplified model reduces its accuracy. Some tentative models may be necessary to reach an acceptable one. However, this is largely compensated by the time that is saved later, during the thermal analysis of other missions and by the confidence that the solution obtained is, at least, close to the best.

Acknowledgment

The authors would like to acknowledge the contribution of Petrônio Noronha de Souza (INPE) in the preparation of the final manuscript.

References

[1] Costello, F. A., Harper, T. P., and Aston, B., "Coating Selection Program," NASA CR-1041, April 1968.

[2] Bettini, R. G., and Costello, F. A., "Optimization of Thermal Systems with Sensitive Optics, Electronics, and Structures," NASA CR-3745, April 1984.

[3] Fragnito, M., Pastena, M., and D'Errico, M., "Spacecraft Thermal Analysis and Control by Thermal Energy Optimum Distribution," *Journal of Spacecraft and Rockets*, Vol. 39, No. 1, 2002, pp. 149–152.

[4] Martin, D., "Parametric Models and Optimization for Rapid Thermal Design," SAE International Paper 2004-01-2273, 2004.

[5] Mareschi, V., Perotto, V., Gorlani, M., Lazzeri, D., and Pin, O., "Application of Stochastic Technique to Spacecraft Thermal and Multidisciplinary Simulations," SAE International Paper 2004-01-2274, 2004.

[6] Herrera, F. L., and Sepúlveda, A. T., "Stochastic Approach to Spacecraft Thermal Control Subsystem," SAE Inc. Paper 2000-01-2484, 2000.

[7] Lamela, F., and Torres, A., "Thermal Analysis Tools for Design and Test Correlation Imposing Objectives," SAE Inc. Paper 2001-01-2408, 2001.

[8] Sousa, F. L., and Ramos, F. M., "Function Optimization Using Extremal Dynamics," ICIPE Paper 2002-015, 2002.

[9] Sousa, F. L., Ramos, F. M., Paglione, P., and Girard, R. M., "New Stochastic Algorithm for Design Optimization," *AIAA Journal*, Vol. 41, No. 9, 2003, pp. 1808–1818.

[10] Sousa, F. L., Ramos, F. M., Galski, R. L., and Muraoka, I., "Generalized Extremal Optimization: A New Meta-heuristic Inspired by a Model of Natural Evolution," *Recent Developments in Biologically Inspired Computing*, edited by L. N. De Castro and F. J. Von Zuben, Idea Group, Inc., Hershey, PA, 2004, pp. 41–60.

[11] Schroder, R., Puls, J., Hajnsek, I., Jochim, F., Neff, T., Kono, J., Paradella, W. R., Silva, M. M. Q., Valeriano, D. M., and Costa, M. P. F., "MAPSAR: A Small L-band SAR Mission for Land Observation," *Acta Astronautica*, Vol. 56, Nos. 1–2, 2005, pp. 35–43.

[12] Tsai, J. R., "Overview of Satellite Thermal Analytical Model," *Journal of Spacecraft and Rockets*, Vol. 41, No. 1, 2004, pp. 120–125.

[13] Bak, P., and Sneppen, K., "Punctuated Equilibrium and Criticality in a Simple Model of Evolution," *Physical Review Letters*, Vol. 71, No. 24, 1993, pp. 4083–4086.

[14] Galski, R. L., Sousa, F. L., Ramos, F. M., and Muraoka, I., "Spacecraft Thermal Design with the Generalized Extremal Optimization Algorithm," IPDO Paper 015, 2004.

[15] Sousa, F. L., Vlassov, V., and Ramos, F. M., "Generalized Extremal Optimization: An Application in Heat Pipe Design," *Applied Mathematical Modelling*, Vol. 28, No. 10, Oct. 2004, pp. 911–931.

[16] Gilmore, D. G., and Collins, R. L., "Thermal Design Analysis," *Satellite Thermal Control Handbook*, edited by D. G. Gilmore, Aerospace Corporation, El Segundo, CA, 1994, pp. 5/21–5/39.

[17] Cardoso, H. P., Muraoka, I., Bastos, J. L. F., Bambace, L. A. W., Oliveira Filho, O. B., and Leite, R. M. G., PCTER Thermal Analysis Software, User's Manual (In Portuguese), INPE, São José dos Campos, SP, Brazil, 1990.

J. Korte
Associate Editor